ADVANCED ENERGY & SUSTAINABILITY RESEARCH
Open Access
www.advenergysustres.com

Optimizing Various Operational Conditions of Hydrazine Single Cell for a Short Stack System

*Jihyeon Park and Jaeyoung Lee**

Although hydrazine fuel cells (HzFCs) have various advantages such as a high theoretical potential, low operating temperature, and no carbon dioxide emission, only a couple of studies on HzFC stack have been reported due to the peculiarity of using an anion exchange membrane and the toxic issue of highly concentrated hydrazine fuel. Herein, how the power output performance in a single-cell system is affected by various operational factors of cell temperature, humidification level, pressurization, fuel concentration, and stoichiometric value is investigated and then a home-made short stack consisting of five single cells (HzFC-5S) to evaluate the difference between the single cell and the stack is built up. Confirmation that the optimization point in the single-cell does not apply to the short stack can be meaningful in accessing its possible commercialization process for portable and mobile devices.

1. Introduction

Because the supply of batteries as an energy source cannot follow up compared to the increased demand for portable/mobile electric machinery, the price of batteries and their components has soared dramatically.[1,2] Direct liquid fuel cells (DLFCs), one of the new types of energy supply systems, are a well-respected field, compensating for the batteries' disadvantages: weight, booming price, and charging time.[3–6] Among various DLFCs, hydrazine fuel cells (HzFCs) applying for an anion exchange membrane (AEM) show as much high power density (1.0–1.2 W cm^{-2}) as hydrogen proton exchange membrane fuel cells (PEMFCs). In addition, HzFCs do not emit carbon dioxide unlike typical direct methanol fuel cells (DMFCs).[7–11] Therefore, HzFCs could be an ecofriendly energy source suitable for small and midterm electronic devices such as scooters, drones, golf carts, and emergency robots.

Many studies are still focusing on the development of hydrazine oxidation electrocatalysts and are limited to the small single-cell application of the developed catalysts.[12–17] Only a couple of studies on operational conditions for HzFCs have been conducted, and even that does not provide sufficient information.[18,19] Even though several fuel cell/stack types of research using a cation exchange membrane (CEM) have been reported, it is difficult to apply them to HzFC/stack using the AEM.[20–26] The difference in the membrane means that the pH condition being operated is different and induces a change in the oxygen reduction reaction (ORR) mechanism. In other words, the ORR mechanism in a cathode part produces water (Equation (1) in acidic media) or consumes water (Equation (2) in alkaline media).

$$O_2 + 4H^+ + 4e^- \rightarrow 2H_2O \tag{1}$$

$$O_2 + 2H_2O + 4e^- \rightarrow 4OH^- \tag{2}$$

Therefore, appropriate cathode humidification could be a critical factor in the HzFC operation. At the same time, since HzFC uses a hydrated hydrazine fuel, water diffusion from the anode part to the cathode part should be considered.

The cell temperature should be controlled carefully between the fuel cell performance and the thermal stability. As AEM has less thermal stability than CEM, it is sensitive to cell temperature which directly affects the fuel cell performance.[27–30] In general, the fuel cell using AEM operates at ≈60 °C, and the fuel cell using CEM operates at around 80–90 °C.

For the energy source of portable devices, fuel cell components are also important.[20] The size of the gas-supplying component varies depending on what kind of gas is injected into the fuel cell among compressed air, pure O_2, and the general atmosphere. A liquid pump as one of the components is also needed to control the fuel flow rate. Under the practical operation,

---

J. Park, J. Lee
School of Earth Sciences and Environmental Engineering
Gwangju Institute of Science and Technology
123 Cheomdangwagi-ro, Buk-gu, Gwangju 61005, South Korea
E-mail: jaeyoung@gist.ac.kr

J. Park
Department of Chemical Engineering
McMaster University
1280 Main St W, Hamilton, Ontario L8S 4L7, Canada

J. Park, J. Lee
Ertl Center for Electrochemistry and Catalysis
Gwangju Institute of Science and Technology
123 Cheomdangwagi-ro, Buk-gu, Gwangju 61005, South Korea

J. Lee
International Future Research Center of Chemical Energy Storage and Conversion Processes
Gwangju Institute of Science and Technology
123 Cheomdangwagi-ro, Buk-gu, Gwangju 61005, South Korea

The ORCID identification number(s) for the author(s) of this article can be found under https://doi.org/10.1002/aesr.202200188.

DOI: 10.1002/aesr.202200188

two-phase contents of N_2H_4 as a liquid fuel and N_2 as a generated gas exist on the anode side, and thus fuel flow rate should be controlled with the consideration of fast removal of the N_2 gas and securement of the reaction time between fuel and catalysts.[31]

In this study, we try to investigate the effect of various operational factors on HzFC performance, including cathode relative humidity, back pressure on the cathode side, cell temperature, fuel concentration of the anodic side, and stoichiometric factor of both sides ($\lambda_{\text{fuel}}/\lambda_{\text{air}}$). Each feature is not independent but rather interdependent on the fuel cell performance. A comprehensive analysis of the HzFC stack, which has a complicated internal structure and large surface area, is accompanied by the reason for the difference in performance with the single cell.

2. Results and Discussion

Standard operation condition is designated for accurate comparison of the fuel cell performance (**Table 1**).

As we mentioned earlier, since alkaline liquid fuel cells consume water on the cathode side and hydrated N_2H_4 fuel on the anode side is supplied, anode water could be already sufficiently supplied to the cathode side through the AEM. In other words, air humidification may not be an essential need at the cathode side. Therefore, we assessed fuel cell performance in terms of air relative humidity adjusting the gas bottle temperature (T_{BT}) and gas preheater temperature (T_{PT}). Another concern is that when humidified air is injected, the gas flow rate just before being supplied to the cell increases because of steam. In addition, the actual reaction process becomes extremely complicated because air, not pure oxygen, is supplied. For example, assuming the dry air condition of 60 °C, 1 atm, and 5000 sccm, 100% humidified air at 60 °C has 0.1524 kg water kg^{-1} dry air from the psychrometric chart. So, the flow rate of N_2, O_2, and H_2O is 3950, 1050, and 1221 sccm, respectively, showing that the total flow rate is increased to 6221 sccm before the gas inlet. That is, it can be confirmed through the simple calculation that when humidifying, not only the partial pressure of oxygen decreases from 0.21 ($O_2/(O_2+N_2)$) to 0.17 ($O_2/(O_2+N_2+H_2O)$), but also increases to the flow rate (5000 → 6221 sccm). Therefore, elements that require humidification and elements that do not require humidification are combined to form the optimal humidification point. Because of these considered elements, we expected that the fuel cell performance is maximized under the particular humidification condition.

Figure 1 shows single-cell performances between 100% humidified air and full dry air. Maximum power densities at a relative humidity of 0, 20, 40, 60, 80, and 100% are 487, 530, 524, 571, 610, and 673 mW cm^{-2}, respectively. We confirmed that relative humidity affected not only the performance of the fuel cell but also the open-circuit voltage (OCV) because of the different overpotentials of ORR. Interestingly, the performance and even OCV are the highest at 100% humidified air. It can be elucidated by a similar CO_2 reduction system using AEM.[32] If there is no moisture in the supplied gas, a diffusion gradient is formed in the gas diffusion layer (GDL) region, which adversely affects performance. On the other hand, the effect of the consumed water on the cathode side could be negligible in sufficient humidification conditions.

Table 1. The standard operation condition of alkaline liquid fuel cell.

Features[a)]	Value	Features	Value
Fuel concentration	4 M	Relative humidity	100%
Stoichiometric factor (λ_{fuel})	9	Cell temperature	60 °C
Stoichiometric factor (λ_{gas})	9	Back pressure	0 bar

[a)] Stoichiometric factors were calculated based on $j = 1000\ \text{mA cm}^{-2}$.

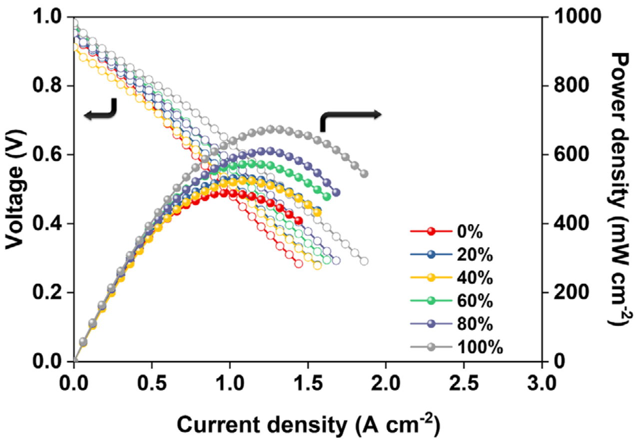

Figure 1. The HzFC performance in the operation of the single cell controlling the relative humidity of the air. The unmentioned test condition except for the relative humidity is the same as the standard condition. Back pressure = 0.0 bar, fuel concentration = 4 M N_2H_4, cell temperature = 60 °C, and $\lambda_{\text{fuel}}/\lambda_{\text{gas}} = 9/9$.

This means that the mentioned elements of consideration may not have a greater impact than expected, and water consumption is actively progressing in the cathode part.

The application of the back pressure pushes air in the perpendicular direction of the GDL, resulting in more contact with the ORR catalyst. However, at the same time, pressurization increases the pressure inside the fuel cell and may cause problems in which fuel or gas leaks through the gasket. To compose the portable liquid fuel cell, the injected gas type should be selected from pure O_2, compressed air, and the general atmosphere, and if proper performance of the fuel cell is exhibited only in compressed air, an increase in weight and volume due to the compressor construction should also be considered. **Figure 2** shows the different polarization curves of a single fuel cell by increasing the back pressure up to 2.0 bar. OCV in all experiments is ≈0.99 V, indicating that OCV is not affected by back pressure at all, since the potential of the fuel cell is irrelevant to the number of reactants. Peak power densities gradually increase as the back pressure increases, from 673 (0 bar) to 929 mW cm^{-2} (2.0 bar). From the absence of back pressure, it is increased by 7–12% each time the back pressure increases by 0.5 bar, and the maximum performance of 929 mW cm^{-2} seems to converge at 2.0 bar, which is presumed to be due to the approach of oxygen density by the limit of the reaction catalyst. Therefore, a portable fuel cell system should be designed in

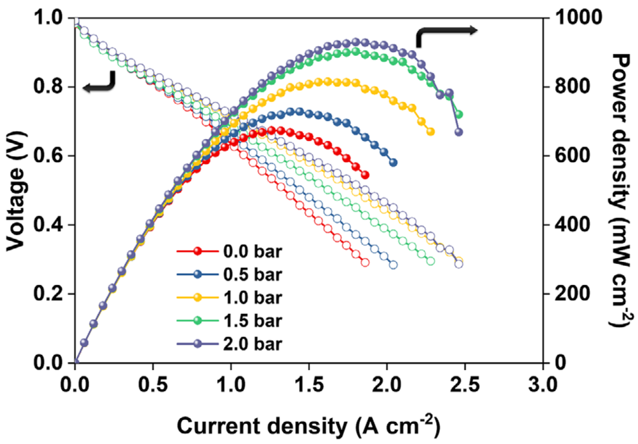

Figure 2. The HzFC performance in the operation of the single cell controlling the back pressure of the air. The unmentioned test condition except for the back pressure is the same as the standard condition. Relative humidity = 100 %, fuel concentration = 4 M N_2H_4, cell temperature = 60 °C, and $\lambda_{\text{fuel}}/\lambda_{\text{gas}} = 9/9$.

both considerations of a performance increase due to the back pressure and an efficiency decrease due to the weight of the compressor construction.

Controlling both fuel concentration and fuel flow rate could be considered in terms of multiple perspectives. The higher the fuel concentration, the smaller the size of the fuel tank of the portable liquid fuel cell, and concentration loss could be observed in a higher current density region when oxygen is sufficient. To control the fuel concentration, we kept the stoichiometric factor of fuel as 9 in all experiments. In addition, to analyze the effect of fuel concentration on the cell performance precisely, the fuel cell operation is conducted from the low concentration to the high concentration. **Figure 3** shows different power performances as a function of the fuel concentration, showing the highest peak power density of 673 mW cm^{-2} at 4.0 M N_2H_4. Because a very high stoichiometric value of 9 is maintained, the performance applying 1.0 M N_2H_4 was relatively low at 238 mW cm^{-2}. It might be due to insufficient contacting fuel reactivity of the catalyst. On the other hand, the reason for the low performance of 483 mW cm^{-2} at 8.0 M might be the slow flow rate and incomplete emission of nitrogen gas. The design of a flow channel for emitting the generated gas will be covered in our future work.

Increasing cell temperature is the simplest way to improve fuel cell performance, but it should be thoroughly considered because the AEM is vulnerable to heat. **Figure 4** shows that cell temperature influences power performance. In this study, at a cell temperature of 80 °C, the maximum peak power density of 773 mW cm^{-2} was observed, whereas the minimum peak power density of 287 mW cm^{-2} was obtained at 100 °C. The increase in fuel cell performance at 70 → 80 °C is relatively lowered compared to that at 60 → 70 °C, and the performance is decreased at 80 °C or more, it being estimated that the thermal resistance of AEM we used is around 80 °C. That's why the fuel cell performance is severely decreased at 100 °C.

The stoichiometric factor is one of the important operational factors of the fuel cell in the efficiency of the fuel cell and the device size. In the case of liquid fuel cells that emphasize portability, which gas is used among oxygen, compressed air, or the general atmosphere is an essential consideration for constituting the equipment of the initial fuel cell system. The lower λ_{air}, the fewer additional devices required, so the compact fuel cell system could be achieved. **Figure 5**a shows the polarization curve of the alkaline liquid fuel cell maintaining λ_{air}. As λ_{fuel} decreases, initial performance (≈1 A cm^{-2}) minutely increases. However when λ_{fuel} is 1.5, the N_2 product gas at the anode side could not be properly emitted, so the peak power density is not observed. Meanwhile, we also conducted the performance test maintaining λ_{fuel} (Figure 5b). Because the generated gas was properly discharged, the peak power density was observed, but it was confirmed that the fuel cell performance decreased as a function of λ_{air}. Figure 5c shows the fuel cell performance when both stoichiometric factors are reduced, keeping the ratio of $\lambda_{\text{fuel}}/\lambda_{\text{air}}$. The

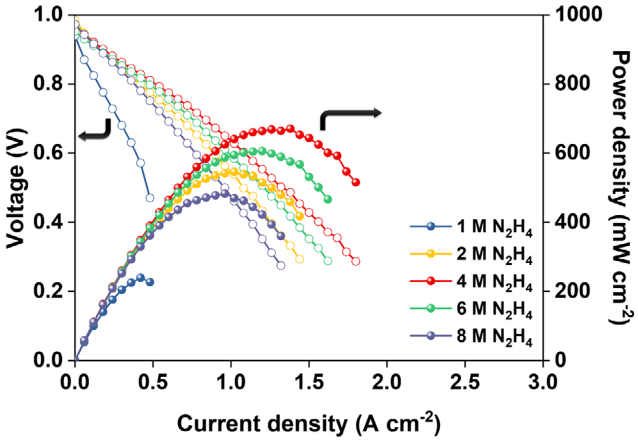

Figure 3. The HzFC performance in the operation of the single cell controlling N_2H_4 concentration of the fuel. The unmentioned test condition except for the fuel concentration is the same as the standard condition. Relative humidity = 100%, back pressure = 0.0 bar, cell temperature = 60 °C, and $\lambda_{\text{fuel}}/\lambda_{\text{gas}} = 9/9$.

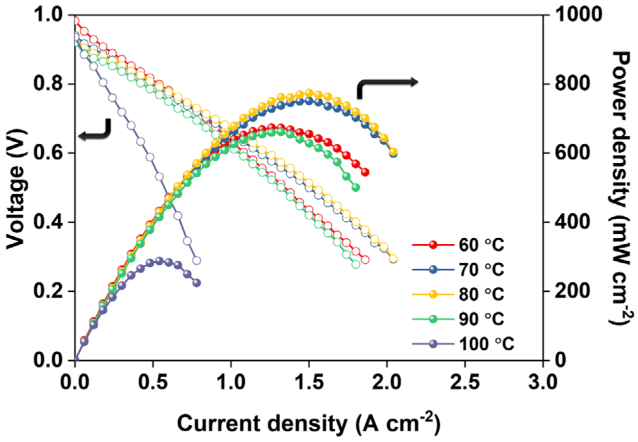

Figure 4. The HzFC performance in the operation of the single cell controlling the cell temperature. The unmentioned test condition except for the cell temperature is the same as the standard condition. Relative humidity = 100%, back pressure = 0.0 bar, fuel concentration = 4 M N_2H_4, and $\lambda_{\text{fuel}}/\lambda_{\text{gas}} = 9/9$.

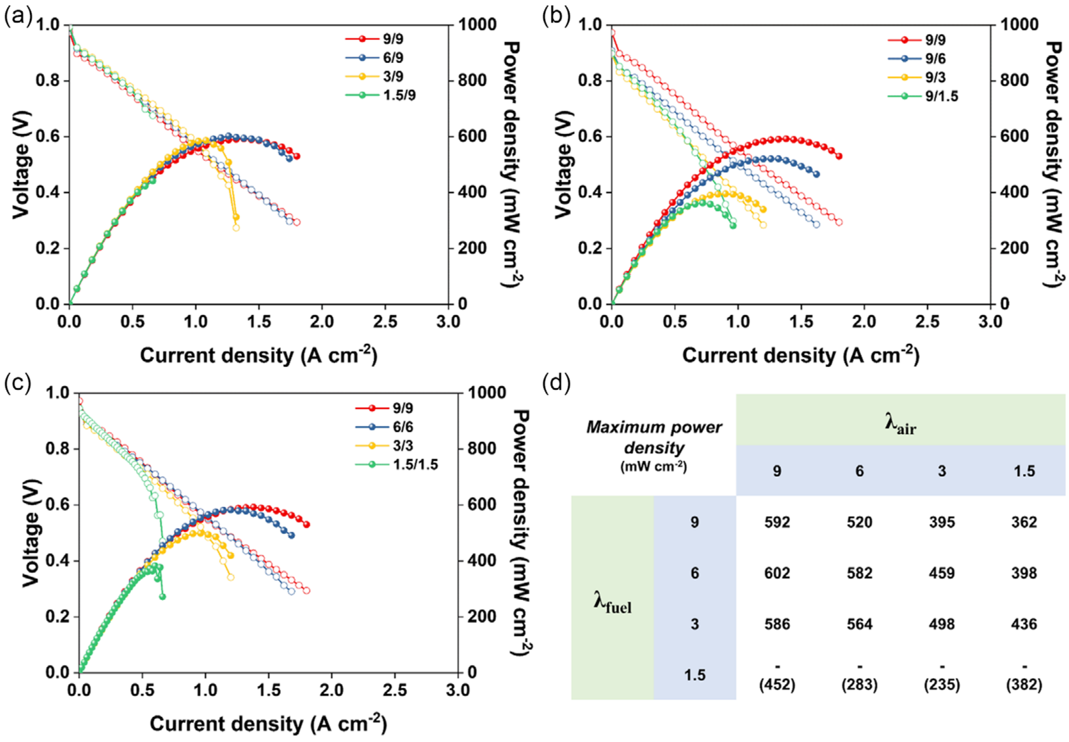

Maximum power density (mW cm-2)		λ_{air}			
		9	6	3	1.5
λ_{fuel}	9	592	520	395	362
	6	602	582	459	398
	3	586	564	498	436
	1.5	- (452)	- (283)	- (235)	- (382)

Figure 5. The HzFC performance in the operation of the single cell controlling stoichiometric factors of a) fuel and b) air. c) The fuel cell performance when both stoichiometric factors are reduced, keeping the ratio of $\lambda_{fuel}/\lambda_{air}$. The order in the graph legend is $\lambda_{fuel}/\lambda_{air}$. d) The peak power density in all conditions. The unmentioned test condition except for the stoichiometric factor is the same as the standard condition. Relative humidity = 100%, back pressure = 0.0 bar, fuel concentration = 4 M N_2H_4, and cell temperature = 60 °C.

same power density is shown under all conditions in the low-current region ($\approx 0.5\ \mathrm{A\,cm^{-2}}$), but the difference in the peak power density was observed in the high-current-density region due to problems such as lack of reactants and slowing down of product emission. The peak power density of all conditions is enumerated in Figure 5d.

Fuel cell efficiency is composed of the product of voltage efficiency ($\varepsilon_{voltage}$), thermodynamic efficiency (ε_{thermo}), and fuel efficiency (ε_{fuel}) (Equation (3)).[33] Especially, HzFC has the advantage because ε_{thermo} of HzFC is even higher than 1, compared to ε_{thermo} of PEMFC (Equation (4)).[34]

$$\mathscr{E}_{FC} = \mathscr{E}_{voltage} \times \mathscr{E}_{thermo} \times \mathscr{E}_{fuel} = \left(\frac{V}{E}\right) \times \left(\frac{\Delta G^0}{\Delta H^0_{HHV}}\right) \times \left(\frac{1}{\lambda_{fuel}}\right) \tag{3}$$

$$\mathscr{E}^{HzFC}_{thermo} = \frac{-623.6\ \mathrm{kJ\,mol^{-1}}}{-622.3\ \mathrm{kJ\,mol^{-1}}} = 1.002$$
$$\mathscr{E}^{PEMFC}_{thermo} = \frac{-237.3\ \mathrm{kJ\,mol^{-1}}}{-286\ \mathrm{kJ\,mol^{-1}}} = 0.83 \tag{4}$$

As shown in Figure 5a, under sufficient air supply conditions, the lower λ_{fuel} (the higher ε_{fuel}), the better the fuel cell performance in the low-current region (≈1 A). However, λ_{fuel} should not be just reduced, because N_2H_4 fuel should be injected excessively to react from the beginning to the end of the flow channel. In addition, the phase transition of fuel inside the fuel cell ($N_2H_{4,\,(l)} \rightarrow N_{2,\,(g)}$) interferes with the catalyst contact of the fuel and makes the flow rate unstable. Therefore, although higher fuel cell efficiency could be achieved, λ_{fuel} cannot be easily reduced.

By referring to the above single-cell measurements, the operational condition of the five-stack HzFC (HzFC-5S) is designed. The preparation of catalysts and membrane electrode assembly (MEA) is the same as those in the single-cell condition except for the size of MEA ($25 \rightarrow 31.5\ \mathrm{cm^2}$). Because the stack does not have heating bars, 100% humidified N_2 gas and DI water heated to 60 °C were supplied for 1 h during the hydration process to increase the initial stack temperature. Besides, the commonly used λ_{air} was fixed as 1.5 (4778 sccm, Equation (5)).[35,36] And λ_{fuel} was fixed as 3.0 based on the highest peak current density at λ_{air} of 1.5 (Figure 5d).

$$\frac{\lambda_{air} \cdot j \cdot A/nF}{P_{O_2}/RT} = \frac{1.5 \cdot 1[\mathrm{A\,cm^{-2}}] \cdot 157.5[\mathrm{cm^2}]/4 \cdot 96485[\mathrm{C\,mol^{-1}}]}{0.21[\mathrm{atm}]/0.082[\mathrm{atm \cdot L\,mol^{-1} \cdot K^{-1}}] \cdot (273.15 + 60)[\mathrm{K}]} \times 60[\mathrm{s\,min^{-1}}] \times 1000[\mathrm{mL\,L^{-1}}] = 4778\ \mathrm{sccm} \tag{5}$$

Figure 6 shows the polarization curve of the HzFC-5S as a function of fuel concentration. Unlike the highest power performance in the fuel concentration of 4 M in the single cell, the HzFC-5S rather showed the highest power performance applying

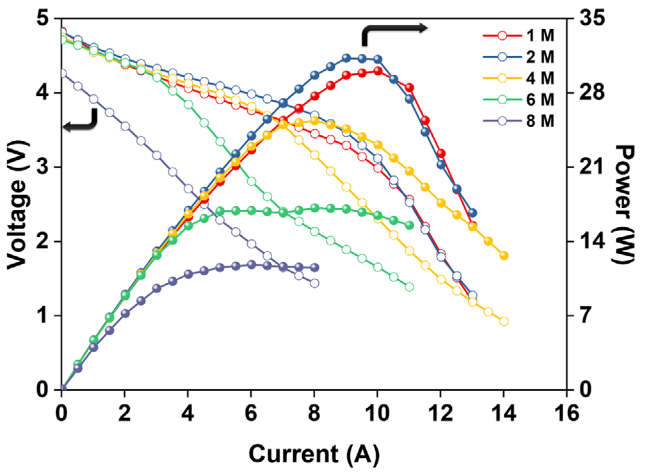

Figure 6. The performance in the operation of the five-stack HzFC controlling N_2H_4 concentration of the fuel. λ_{fuel} and λ_{air} are 3 and 1.5, respectively, based on the current density of 1000 mA cm^{-2} and the active area of 157.5 cm^2 (31.5 cm^2 × 5).

the lower fuel concentration of 2 M. This result shows when a low concentration of N_2H_4 fuel is supplied at a high flow rate, the generated N_2 gas can be easily emitted out. So the generated gas emission in the stack operation is much more important than in the single-cell operation.

The OCV of the HzFC-5S in the series circuit is ≈4.8 V, so the effect on the fuel crossover seems to be weak. However, the peak power density of the HzFC-5S in 2 M is around 200 mW cm^{-2} (at the stack power of 31 W), which is even 50% lower than the single-cell performance of 436 mW cm^{-2} in 2 M under the same condition ($\lambda_{\text{fuel}}/\lambda_{\text{air}} = 3/1.5$).

To confirm the inherent full power of HzFC-5S, we changed the stack test condition to O_2 atmosphere and observed the maximum stack power of around 100 W (**Figure** 7a). The result shows that if sufficient fuel and oxidant are supplied to the stack, the overall performance could be improved. However, there is a cell temperature issue in the stack that was not observed in single cell. When the cell temperature is high, the reaction rate and ion diffusivity increase, thereby positively increasing the fuel cell performance and negatively damaging the AEM. In the case of the single cell, which maintains the cell temperature of 80 °C via heating bars, the maximum variation of temperature is 3 °C during the operation (Figure 7b), whereas in the case of the stack, which heats as the exothermic reaction is easily accumulated, the temperature rises almost 20 °C from the lowest 77 °C to the highest 97 °C even if there are air-cooling fans (Figure 7c). It should be noted that heat management is possible through fuel concentration. A fast flow rate of a low concentration of fuel is effective

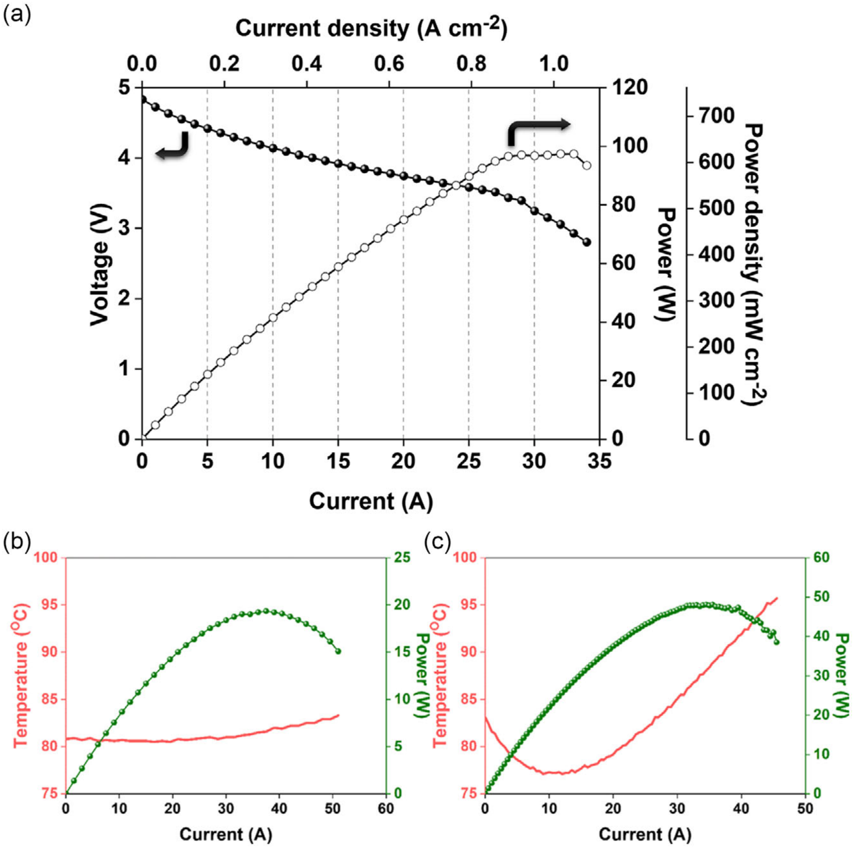

Figure 7. a) The performance in the operation of the HzFC-5S under pure O_2 atmosphere. The power performance and temperature variance in the operation of b) the single-cell HzFC at 80 °C in the MEA size of 25 cm^2 and c) the three-stack HzFC at 80 °C in total MEA size of 94.5 cm^2. The gas atmosphere is air and pure O_2 at the single cell and the stack, respectively, with the same $\lambda_{\text{fuel}}/\lambda_{\text{gas}}$ of 9/6.

to remove the accumulated heat inside the stack, but a slow flow rate of a high concentration of fuel is relatively vulnerable to controlling the cell temperature.

3. Conclusion

The gap between a half-cell measurement of each component and a single-cell operation considering various experimental conditions should be intensively analyzed to develop the stack for emerging delivering devices/systems. We showed that the performance change of the single cell could be constructed by various operational parameters such as relative humidity, back pressure, cell temperature, fuel concentration, and stoichiometric factors. It is quite encouraging to show around 100 W power of the short-stack HzFC. There are still a couple of hurdles that should be overcome for fuel application; we discussed various operational perspectives of alkaline liquid fuel cells. To jump from the laboratory research stage to the empirical research stage, other operational components such as the compressor, the liquid pump, the gas blower, the fuel/water tank, and the flow channel design should also be considered for the practical fuel cell/stack.

4. Experimental Section

6.6 g of nickel chloride ($NiCl_2$, 98%, Sigma-Aldrich) and 3.0 g of polyvinylpyrrolidone (PVP, 10 000 g mol^{-1}, Sigma-Aldrich) were dissolved in 1.0L of ethylene glycol (EG, Sigma-Aldrich). 1.0 g of carbon support (Vulcan XC-72) was added to a green solution after stirring. 1.0 M NaOH was added into the mixed solution until pH 10. Reflux and distillation in processing the conventional polyol reduction method were applied at 160 °C for 4 h. Centrifugation was carried out three times with deionized (DI) water to remove the unreacted materials. Then, the catalyst slurry was filtered with DI water. Synthesized catalyst slurry was dried in an oven at 60 °C for 24 h. At last, the dried sample was annealed at 300 °C for under the 4% hydrogen contained in Ar. Ni/C catalyst of anode catalyst for HzFC contained 45–50 wt% of Ni metal on the carbon support. The cathode catalyst was the commercial Pt/C (46.7%, Tanaka).

Catalyst ink was prepared with each catalyst powder, nPA, and 10% Nafion ionomer solution. Nafion ionomer was used at 5% versus the catalyst weight.[7,8] The ink mixture was ultrasonicated in an ice bath for 1.0 h. The sonicated ink was air sprayed on AvCarb MGL 190 for the anode electrode and Sigracet 29 BC for the cathode electrode, respectively. The loading amounts of the catalyst at the anode and cathode were 1.6 $mg_{Cat}\,cm^{-2}$ and 1.0 $mg_{Pt}\,cm^{-2}$, respectively. The MEA was fabricated by pressing at 60 °C with both sprayed electrodes and a lab-made AEM.[7] The size of MEA was 25.0 cm^2 for a single cell and 31.5 cm^2 for a bipolar plate of the stack, respectively.

Before the single-cell test, DI water and 100% humidified N_2 were injected into the anode line and the cathode line, respectively, for the hydration of MEA. Operation conditions such as cell temperature, the concentration of hydrazine fuel, back pressure, stoichiometric factors ($\lambda_{fuel}/\lambda_{gas}$), and relative humidity were differently applied in the single-cell test. The stoichiometric factor and relative humidity were calculated by Equation (6) and (7), respectively.[37]

$$\lambda = \frac{\text{flow rate of supplied reactant}}{j \cdot A/nF} \qquad (6)$$

$$\mathrm{RH} = \left(e^{\frac{17.625\times T_{BT}}{243.04+T_{BT}} - \frac{17.625\times T_{PT}}{243.04+T_{PT}}}\right) \times 100(\%) \qquad (7)$$

where j is current density, A is MEA area, n is the number of electrons, and F is the Faradaic constant. RH, T_{BT}, and T_{PT} represent relative humidity, the gas bottle temperature, and the gas preheater temperature, respectively.

Both the HzFC single cell and stack consisted of graphite bipolar plates, 0.3 mm PTFE gaskets, gold-coated copper current collectors, and aluminum endplates (see Figure S1a,b, Supporting Information). The flow field pattern of bipolar plates was four-channel serpentine and the active electrode area was 25 cm^2 (single-cell)/31.5 cm^2 (stack). The feed flow through the single cell/stack was U shaped, where the inlet downside for liquid fuel and outlet upside for gas products with the unreacted liquid fuel were located on the same side, considering the phase transition of reactants and gravity effect. After stacking the prepared MEAs and bipolar plates in layers, the HzFC single cell/stack was completely assembled with a force of 60 kgf·m.

All performances of the HzFC single cell/stack were obtained through the polarization curve. The single cell was tested with heating bars to control the cell temperature, whereas the stack was operated with air-cooling fans due to an excessive exothermic reaction. After the hydration process with DI water and 100% humidified N_2 for 1.0 h, the test was conducted after the circulation of fuel/oxygen until the resistance of each MEA reached 10 mΩ or less. The turn voltage of single cell and stack was 0.3 and 1.5 V, respectively. Figure S1c, Supporting Information, shows a photograph of the HzFC stack during the operation.

Supporting Information

Supporting Information is available from the Wiley Online Library or from the author.

Acknowledgements

This research was supported by the National R&D Program through the National Research Foundation of Korea (NRF), funded by the Ministry of Science and ICT (NRF-2021K1A4A8A01079455) and this research was supported by the Korea Institute of Energy Technology Evaluation and Planning (KETEP) granted financial resources from the Ministry of Trade, Industry & Energy, Republic of Korea (No. 20213030040590).

Conflict of Interest

The authors declare no conflict of interest.

Data Availability Statement

The data that support the findings of this study are available from the corresponding author upon reasonable request.

Keywords

alkaline liquid fuel cells, driving conditions, hydrazine, operational controls, stack performances

Received: November 26, 2022
Revised: December 24, 2022
Published online: January 17, 2023

---

[1] C. Grosjean, P. H. Miranda, M. Perrin, P. Poggi, *Renewable Sustainable Energy Rev.* **2012**, *16*, 1735.
[2] G. Martin, L. Rentsch, M. Höck, M. Bertau, *Energy Storage Mater.* **2017**, *6*, 171.

[3] K. Scott, P. Argyropoulos, K. Sundmacher, *J. Electroanal. Chem.* **1999**, *477*, 97.
[4] B. C. Ong, S. K. Kamarudin, S. Basri, *Int. J. Hydrogen Energy* **2017**, *42*, 10142.
[5] W. Qian, D. P. Wilkinson, J. Shen, H. Wang, J. Zhang, *J. Power Sources* **2006**, *154*, 202.
[6] K. Tran, T. Q. Nguyen, A. M. Bartrom, A. Sadiki, J. L. Haan, *Fuel Cells* **2014**, *14*, 834.
[7] S. Bae, J. Park, Y. Hwang, J.-S. Park, J. Lee, B. Jeong, *J. Energy Chem.* **2022**, *64*, 276.
[8] J. Park, S. Bae, J.-S. Park, S. Bong, J. Lee, *ACS Appl. Nano Mater.* **2021**, *4*, 8145.
[9] D. Khalafallah, M. Zhi, Z. Hong, *ChemCatChem* **2021**, *13*, 81.
[10] Z. Lu, M. Sun, T. Xu, Y. Li, W. Xu, Z. Chang, Y. Ding, X. Sun, L. Jiang, *Adv. Mater.* **2015**, *27*, 2361.
[11] Y. Yan, J.-Y. Zhang, X.-R. Shi, Y. Zhu, C. Xia, S. Zaman, X. Hu, X. Wang, B. Y. Xia, *ACS Nano* **2021**, *15*, 10286.
[12] T. Wang, Q. Wang, Y. Wang, Y. Da, W. Zhou, Y. Shao, D. Li, S. Zhan, J. Yuan, H. Wang, *Angew. Chem.* **2019**, *131*, 13600.
[13] G. Wang, J. Chen, P. Cai, J. Jia, Z. Wen, *J. Mater. Chem. A* **2018**, *6*, 17763.
[14] J. Ding, P. Kannan, P. Wang, S. Ji, H. Wang, Q. Liu, H. Gai, F. Liu, R. Wang, *J. Power Sources* **2019**, *413*, 209.
[15] T. Zhang, T. Asefa, *Adv. Mater.* **2019**, *31*, 1804394.
[16] Q. Qian, J. Zhang, J. Li, Y. Li, X. Jin, Y. Zhu, Y. Liu, Z. Li, A. El-Harairy, C. Xiao, G. Zhang, Y. Xie, *Angew. Chem.* **2021**, *133*, 6049.
[17] K. Ojha, E. M. Farber, T. Y. Burshtein, D. Eisenberg, *Angew. Chem. Int. Ed.* **2018**, *57*, 17168.
[18] K. Asazawa, T. Sakamoto, S. Yamaguchi, K. Yamada, H. Fujikawa, H. Tanaka, K. Oguro, *J. Electrochem. Soc.* **2009**, *156*, B509.
[19] H. Hwang, S. Hong, D.-H. Kim, M.-S. Kang, J.-S. Park, S. Uhm, J. Lee, *J. Energy Chem.* **2020**, *51*, 175.
[20] D. Kim, J. Lee, T.-H. Lim, I.-H. Oh, H. Y. Ha, *J. Power Sources* **2006**, *155*, 203.
[21] M. R. Andrew, W. J. Gressler, J. K. Johnson, R. T. Short, K. R. Williams, *J. Appl. Electrochem.* **1972**, *2*, 327.
[22] J.-Y. Park, Y. Seo, S. Kang, D. You, H. Cho, Y. Na, *Int. J. Hydrogen Energy* **2012**, *37*, 5946.
[23] D. Buttin, M. Dupont, M. Straumann, R. Gille, J.-C. Dubois, R. Ornelas, G. P. Fleba, E. Ramunni, V. Antonucci, A. S. Aricoá, P. Cretiá, E. Modica, M. Pham-Thi, J.-P. Ganne, *J. Appl. Electrochem.* **2001**, *31*, 275.
[24] Y. Liu, X. Xie, Y. Shang, R. Li, L. Qi, J. Guo, V. K. Mathur, *J. Power Sources* **2007**, *164*, 322.
[25] H. Joh, S. Hwang, J. Cho, T. Ha, S. Kim, S. Moon, H. Ha, *Int. J. Hydrogen Energy* **2008**, *33*, 7153.
[26] K. Scott, W. M. Taama, P. Argyropoulos, *J. Power Sources* **1999**, *79*, 43.
[27] Z. Pan, H. Zhuang, Y. Bi, L. An, *J. Power Sources* **1999**, *79*, 43.
[28] A. M. Bartrom, J. L. Haan, *J. Power Sources* **2012**, *214*, 68.
[29] S. Hong, S. Chung, J. Park, J. P. Hwang, C. H. Lee, S. Uhm, S. Bong, J. Lee, *ACS Catal.* **2021**, *11*, 4722.
[30] R. C. Raimundo, J. V. C. Vargas, J. C. Ordonez, W. Balmant, P. T. B. Polla, A. B. Mariano, C. E. B. Marino, *Int. J. Hydrogen Energy* **2020**, *45*, 5723.
[31] Y.-C. Park, D.-H. Peck, S.-K. Dong, S.-K. Kim, S. Lim, D.-H. Jung, J.-H. Jang, D.-Y. Lee, *Int. J. Hydrogen Energy* **2011**, *36*, 1853.
[32] W. Choi, S. Park, W. Jung, D. H. Won, J. Na, Y. J. Hwang, *ACS Energy Lett.* **2022**, *7*, 939.
[33] R. O'Hayre, S.-W. Cha, W. Colella, F. B. Prinz, *Fuel Cell Fundamentals*, John Wiley & Sons, Hoboken NJ **2016**.
[34] P. Vanysek, *CRC Handbook of Chemistry and Physics* (Ed: W. M. Haynes), 97th ed., Vol. *8*, CRC Press **2016**, p. 1, https://doi.org/10.1201/9781315380476.
[35] D. Candusso, F. Harel, A. De Bernardinis, X. François, M. C. Péra, D. Hissel, P. Schott, G. Coquery, J.-M. Kauffmann, *Int. J. Hydrogen Energy* **2006**, *31*, 1019.
[36] N. Dyantyi, A. Parsons, C. Sita, S. Pasupathi, *Open Eng.* **2017**, *7*, 287.
[37] O. A. Alduchov, R. E. Eskridge, *J. Appl. Meteorol. Climatol.* **1996**, *35*, 601.